

Off-resonance magnetic resonance angiography improves visualization of in-stent lumen in peripheral nitinol stents compared to conventional T1-weighted acquisitions: an in vitro comparison study

Gitsios Gitsioudis¹ · Philipp Fortner¹ · Matthias Stuber^{2,3} · Anna Missiou¹ · Florian Andre¹ · Oliver J. Müller¹ · Hugo A. Katus¹ · Grigorios Korosoglou¹

Received: 10 March 2016 / Accepted: 2 August 2016 / Published online: 17 August 2016
© Springer Science+Business Media Dordrecht 2016

Abstract To compare the value of inversion recovery with on-resonant water suppression (IRON) to conventional T1-weighted (T1w) MRA and computed tomography angiography (CTA) for visualization of peripheral nitinol stents. We visualized 14 different peripheral nitinol stents in vitro both using Gadolinium (Gd) and ultrasmall superparamagnetic iron nanoparticles (USPIOs) for conventional T1w and IRON-MRA using clinical grade 1.5T MR scanner and iodinated contrast material for CTA using a 256-slice CT scanner. Parameter assessment included signal- and contrast-to-noise ratio (S/CNR), relative in-stent signal and artificial lumen narrowing. X-ray angiography served as gold standard for diameter assessment. Gd-enhanced IRON-MRA exhibited highest in-stent SNR and CNR values compared to conventional T1w MRA (IRON (Gd/USPIO): SNR = $30 \pm 3/21 \pm 2$, CNR = $23 \pm 2/14 \pm 1$; T1w: SNR = $16 \pm 1/14 \pm 2$, CNR = $12 \pm 1/10 \pm 1$, all $p < 0.05$). Furthermore, IRON-MRA achieved highest relative in-stent signal both using Gd and USPIO (IRON (Gd/

USPIO): $121 \pm 8\%/103 \pm 6\%$; T1w: $73 \pm 2\%/66 \pm 4\%$; CTA: $84 \pm 6\%$, all $p < 0.05$). However, artificial lumen narrowing appeared similar in all imaging protocols (IRON (Gd/USPIO): $21 \pm 3\%/21 \pm 2\%$; T1w: $16 \pm 4\%/17 \pm 3\%$; CTA: $19 \pm 2\%$, all $p = \text{NS}$). Finally, IRON-MRA provided improvement of the in-stent lumen visualization with an ‘open-close-open’ design, which revealed a complete in-stent signal loss in T1w MRA. IRON-MRA improves in-stent visualization in vitro compared to conventional T1w MRA and CTA. In light of the in vitro results with Gd-enhanced IRON-MRA, the clinical implementation of such an approach appears promising.

Keywords Magnetic resonance angiography (MRA) · Inversion recovery with on-resonant water suppression (IRON) · T1-weighted MRA · Stent-related artifacts · Computed tomography angiography (CTA)

Introduction

Peripheral artery disease (PAD) is the third leading cause of cardiovascular morbidity in the industrialized countries [1]. Endovascular interventions continuously gain importance for the treatment of symptomatic PAD [2, 3]. Mid and long-term complications such as neo-intimal hyperplasia causing restenosis and thrombotic vessel occlusion implicate the necessity of serial non-invasive assessment.

Duplex ultrasound is the first-line imaging modality for the assessment of PAD according to current guidelines [4]. Major limitations with duplex ultrasound are (i) high operator dependence, (ii) difficulties with imaging crural and aorto-iliac arteries and (iii) simultaneous acquisition of a long vascular segment and putting it in the visual context of adjacent segments [5]. On the other hand, computed

Electronic supplementary material The online version of this article (doi:10.1007/s10554-016-0955-4) contains supplementary material, which is available to authorized users.

✉ Gitsios Gitsioudis
gitsioudis_correspondence@web.de

¹ Clinic of Internal Medicine, Department of Cardiology, University of Heidelberg, Im Neuenheimer Feld 410, 69120 Heidelberg, Germany

² Russell H. Morgan Department of Radiology and Radiological Sciences, Division of MR Research, Johns Hopkins University School of Medicine, Baltimore, MD, USA

³ Center for Biomedical Imaging (CIBM), University Hospital Lausanne, Lausanne, Switzerland

tomography angiography (CTA) provides high diagnostic accuracy, but requires administration of iodinated contrast material [6] and exposure to ionizing radiation which may limit its serial applicability [7]. Above, extensive vascular calcification significantly impacts on its diagnostic accuracy [8, 9]. In contrast, magnetic resonance angiography (MRA) enables for robust assessment of vascular anatomy without the need of ionizing radiation [10]. However, stent-related artifacts in MRA arising from susceptibility and radiofrequency effects may limit stent visualization [11–15]. Inversion recovery with on-resonant water suppression (IRON) enables for visualization of susceptibility-induced off-resonant protons with positive signal and was shown to improve vessel delineation in prior investigations [16–18].

In the present study we therefore sought to assess the value of IRON-MRA in comparison to conventional T1-weighted (T1w) MRA and CTA for the in vitro visualization of peripheral nitinol stents using Gadolinium (Gd) and ultrasmall superparamagnetic nanoparticles (USPIOs) as contrast material.

Materials and methods

Stents and in vitro model

We evaluated a total of 14 different nitinol vascular stents in vitro, which were expanded in polyethylene tubes to nominal diameters from 6 to 11 mm (Table 1). The stented tubes were placed in a plastic box (140×140×70 mm)

filled with normal saline solution with an initial temperature of 37°C to ensure complete stent expansion. To compare MRA images with CTA we designed a static in vitro model and applied scan mode settings as previously described [19].

Conventional X-ray angiography

Conventional X-ray angiography was performed using a C-arm angiographic system (Allura System, Philips Medical Systems, Best, The Netherlands) and served as the gold standard for diameter assessment. X-ray images were acquired in AP position (0°–0°) with source-image distance of 87 cm, field diameter 25 cm, tube voltage of 60 kV and tube current of 50 mA. The diameter of each stent after balloon inflation was calculated on the basis of a radiopaque reference scale that was simultaneously imaged by X-ray with the stented tube. This diameter (D_{Xray}) was calculated using dedicated medical imaging software OsirixMD (Osirix MD v.2.8). All diameter measurements were performed blinded to the results from MRA and CTA.

Magnetic resonance angiography (MRA)

All MRA images were acquired in a clinical 1.5T scanner (Intera Achieva; Philips Healthcare, Best, The Netherlands) using a 32-element cardiac phased-array receiver coil. For all imaging procedures, volume shimming was used. Scans were performed without parallel imaging. To evaluate the impact of stent orientation, all stents were imaged at 0°, 30°, 60° and 90° relative to the static magnetic field B_0 .

Table 1 Technical properties of all analyzed nitinol stents

Abbrev.	Trade name	Manufacturer	Stent design	Nominal stent length (mm)	Diameter nominal (mm)	Diameter D_{Xray} (mm)
CI930	Cristallo ideale	Invatec	Open-close-open	30	9	8.4
CI1130	Cristallo ideale	Invatec	Open-close-open	30	11	9.4
CI940	Cristallo ideale	Invatec	Open-close-open	40	9	7.7
PP1130	Precise Pro RX	Cordis	Open	30	9	8.7
PP830	Precise Pro RX	Cordis	Open	30	8	7.9
SC760	SMART control	Cordis	Open	60	7	5.9
LS730	FlexStar	Edwards	Open	30	7	5.9
A760	Astron	Biotronic	Open	60	7	5.9
A830	Astron	Biotronic	Open	30	8	7.8
LS880	Vascular	Bard	Open	80	8	7.8
V6840	ViVEXX	Bard	Open	40	6–8	5.2
AL71040	Acculink	Abbott	Open	40	7–10	6.1
AL71030	Acculink	Abbott	Open	30	7–10	6.0
AL6830	Acculink	Abbott	Open	30	6–8	4.9

D_{Xray} indicates the in-stent diameter as assessed by X-ray angiography

Assessment of optimal concentration of contrast material for MRA

To investigate the optimum concentration for conventional T1w and IRON-MRA we systematically tested a stepwise increase of intraluminal concentrations between 0 and 20 $\mu\text{mol/ml}$ for gadolinium-DTPA (Gd; Magnevist, Berlex, NJ, USA) and ultrasmall superparamagnetic nanoparticles (USPIOs; P904, Guerbet, Villepinte, France) contrast material in non-stented tubes (Supplementary Fig. 1).

Conventional T1w MRA

For conventional T1w MRA three-dimensional gradient-echo (fast-field-echo, FFE) images were obtained using the following parameters [17]: repetition time/echo time (TR/TE) = 6.1/2.2 ms, flip angle (FA) = 30°, field-of-view (FOV) was adjusted to the stent length as appropriate to achieve full stent coverage (55–100 \times 21 \times 55 mm) and acquired voxel size 0.86 \times 0.6 \times 1.6 mm³. The total scan duration was 14 s.

IRON-MRA

All IRON-MRA acquisitions were acquired based on gradient-echo sequences. For Gd-enhanced IRON-MRA, an on-resonant frequency-selective suppression prepulse with bandwidth_{IRON} (BW_{IRON}) of 100 Hz, a duration of $\tau = 25$ ms and an excitation angle α_{IRON} of 120° was used, as described previously [17]. Conventional fat saturation was achieved by applying a prepulse preceding the IRON prepulse with a –220 Hz frequency offset, a 100 Hz bandwidth, and a 105° FA. Imaging parameters were: TR/TE = 6.0/2.0 (29/2.8) ms, FA = 120° (100°), FOV was adjusted to the stent length as appropriate to achieve full stent coverage (55–100 \times 21 \times 55 mm) and acquired voxel size = 0.86 \times 0.6 \times 1.6 mm³. Following parameters were used for USPIO-enhanced IRON-MRA: $\tau = 10$ ms; TR/TE = 29/2.8 ms; FA = 100°. The total scan duration was 136 s.

MRA image analysis

MRA data sets were analyzed in a random order using Soap-bubble software tool (Release 5.1 for PRIDE V4.*+V5, Philips Healthcare, Best The Netherlands) [20]. Visual analysis was assessed in coronal orientation and included the evaluation of (i) in-stent visualization and the appearance of the (ii) stent ends and (iii) stent struts. Signal- and contrast-to-noise ratios (S/CNR) were calculated in vitro by placing regions of interest (ROIs) in the background, in the in- and out-stent lumen and in adjacent saline solution using original, reformatted magnitude images (Supplementary Fig. 2). Care was taken to standardize ROI size and

placement for better comparison between image sets. The size of the ROI in arbitrary units was 46 ± 3 for ROIs placed in the non- and stented tubes, 1680 ± 320 for ROIs placed in the adjacent saline solution and 1200 ± 150 for ROIs placed in the background. In-stent lumen was divided in three sub-segments: one middle and two adjacent lateral subsegments covering the stent ends (Supplementary Fig. 2). Signal of the non-stented tube (SI_{Tube}) and in-stent signal ($SI_{\text{In-Stent}, i}$, $i = 1, 2, 3$) was measured in axial orientation. $SI_{\text{In-Stent}}$ was assessed for all three in-stent subsegments, and mean value was calculated. The resulting mean value of $SI_{\text{In-Stent}}$ served for subsequent SNR, CNR and relative in-stent signal (RIS) calculations. In-stent diameters were also assessed in all three in-stent subsegments and mean value was calculated ($D_{\text{In-Stent}}$). Artificial lumen narrowing (ALN) was defined as the difference between the in-stent diameter as assessed by X-ray angiography (D_{Xray}) and the diameter in MRA ($D_{\text{In-Stent}}$). All diameters were measured visually using the workstation's software (ViewForum, Philips Medical Systems, Best, The Netherlands). SNR, CNR, RIS and ALN were calculated using the following equations [11, 20]:

$$\text{SNR} = (SI_{\text{In-stent}}) / \text{SDEV}_{\text{Air}} \quad (1.1)$$

$$\text{CNR} = (SI_{\text{In-stent}} - SI_{\text{Adjacent_Solution}}) / \text{SDEV}_{\text{Air}} \quad (1.2)$$

$$\text{RIS}(\%) = (SI_{\text{In-stent}} / SI_{\text{Tube}}) \times 100\% \quad (1.3)$$

$$\text{ALN}(\%) = (D_{\text{Xray}} - D_{\text{In-Stent}}) / D_{\text{Xray}} \times 100\% \quad (1.4)$$

Two blinded experts performed all measurements and calculations.

Computed tomography angiography (CTA)

All CTA acquisitions were performed using a standardized imaging protocol in a clinical 256-slice CT-scanner (Brilliance iCT, Philips Healthcare, Cleveland, OH, USA). The following parameters were used: helical scan mode, collimation = 128 \times 0.625 mm, pitch = 0.18, tube rotation time = 330 ms, FOV 180 mm, effective tube current = 400 mAsec, tube voltage = 120 kV, field-of-view = 180 mm, matrix = 512 \times 512, slice thickness = 0.67 mm, artificial ECG-gating (60/min) with retrospective reconstruction at 75%, dedicated stent convolution kernels (XCD), window width = 1200 HU, window level = 300 HU. Stented tubes were placed parallel to the z-axis of the scanner. Tubes were filled with diluted iodinated contrast material (Ultravist 370, Bayer Schering Pharma AG, Berlin, Germany). As described previously for this in vitro model, dilution was realized with a volume part ratio of 3:100 for iodinated contrast medium and physiologic saline solution (0.9%) respectively, resulting in a fluid with a mean attenuation of 200 HU, which

is consistent with the values obtained in the early arterial phase of CTA clinically [19, 21, 22].

CTA image analysis

CTA data sets were analyzed in a random order using commercially available software (Philips Extended Brilliance Workspace 4.0) as described for MRA. Two experts who were blinded to the MRA results performed all CTA evaluations.

Statistical analysis

Data are presented as mean \pm standard error of mean (SEM). Differences between any two groups (SNR, CNR, RIS and ALN) were compared by Student's *t* test for continuous variables. Continuous variables between more than two groups were compared by one-way ANOVA with post hoc analysis with Bonferroni adjustment for multiple comparisons. Correlation analysis was performed for SNR and CNR with stent diameter and stent length. Calculations were performed using statistical software (MedCalc Software, Version 11.4.2.0, Mariakerke, Belgium). For assessment of inter- and intra-observer variability 20 randomly selected cases were analyzed by two independent observers in terms of SNR and diameter assessment. Readings were separated by 4 weeks to minimize recall bias and deviations from the initial measurements were calculated (%). Differences were considered statistically significant at $p < 0.05$.

Results

Stent visualization and signal quantification

Based on preliminary experiments (Supplementary Fig. 1), we used concentrations of 2 $\mu\text{mol/ml}$ for Gd and USPIO in order to achieve comparable signal level for further comparison of T1w and IRON-MRA. Overall, we comprehensively visualized 14 different nitinol vascular stents in vitro by (i) conventional X-ray angiography, (ii) CTA, (iii) conventional T1w and (iv) IRON-MRA with good image quality. Figure 1 illustrates an overview of representative images for all stent phantoms. Visual analysis of stent-related artifacts is provided in the Supplementary Table 1. With IRON-MRA, SNR and CNR remained constant or even increased within the in-stent segments, whereas conventional T1w MRA and CTA revealed a decrease of in-stent SNR and CNR (Fig. 2a, b). Focusing on the stented subsegments IRON-MRA in conjunction with both Gd and USPIOs exhibited higher SNR, CNR and RIS values compared to conventional T1w MRA (Fig. 2c, e). IRON-MRA in conjunction with Gd provided the highest SNR, CNR

and RIS values, even when compared to CTA (Fig. 2c, e). On the other hand, ALN was similar for all tested modalities (Fig. 2f).

Stent orientation

Nitinol stents presented differences in their appearance on both T1w and IRON-MRA images depending on their orientation relative to the static magnetic field B_0 (representative images for the Invatec and Cordis stents presented in Fig. 3a). IRON-MRA in conjunction with Gd and USPIO provided higher SNR, CNR and RIS values compared to T1w MRA acquisitions for all tested stent orientations (Fig. 3b–d). Increase of SNR, CNR and RIS for stent orientations at 30° and 60° compared to 0° and 90° was observed with Gd- and USPIO-enhanced IRON-MRA images, whereas values remained constant with different stent orientations for the conventional T1w MRA images. No significant difference was detected for ALN change with orientation on MRA (Fig. 3e).

Impact of stent geometry and design on stent visualization

Geometry

SNR and CNR within the stents increased with decreasing diameters both in conventional T1w and IRON-MRA (T1w: SNR: $r = -0.44$, CNR: $r = -0.40$, $p < 0.001$ for both; IRON: SNR: $r = -0.27$, CNR: $r = -0.29$, $p = 0.005$ for both). Furthermore, SNR and CNR increased with increasing stent length for conventional T1w but not for IRON-MRA (T1w: SNR: $r = 0.51$, CNR: $r = 0.46$, $p < 0.001$ for both; IRON: SNR: $r < 0.01$, CNR: $r < 0.01$, $p = \text{NS}$ for both).

Design

To evaluate the role of stent design for in-stent signal attenuation, we tested two stent configurations (i) 'open-close-open' and (ii) 'open' (Table 1). By visual analysis, stents with an 'open' configuration exhibited very good in-stent visualization, whereas stents with an 'open-close-open' design presented an almost complete signal loss of the mid in-stent tube segment in conventional T1w MRA. In contrast, IRON-MRA improved in-stent visualization in the 'open-close-open' stent group, enabling for adequate lumen assessment throughout the entire length of the stent phantom. Furthermore, IRON-MRA provided 3.6/3.7-fold higher SNR/CNR in conjunction with Gd ($p < 0.0001$ for both) and 2.9/2.7-fold higher SNR/CNR in conjunction with USPIOs compared to conventional T1w MRA ($p \leq 0.001$ for both) in stents with 'open-close-open' configuration (Fig. 4a, b). Finally, IRON-MRA improved RIS and ALN

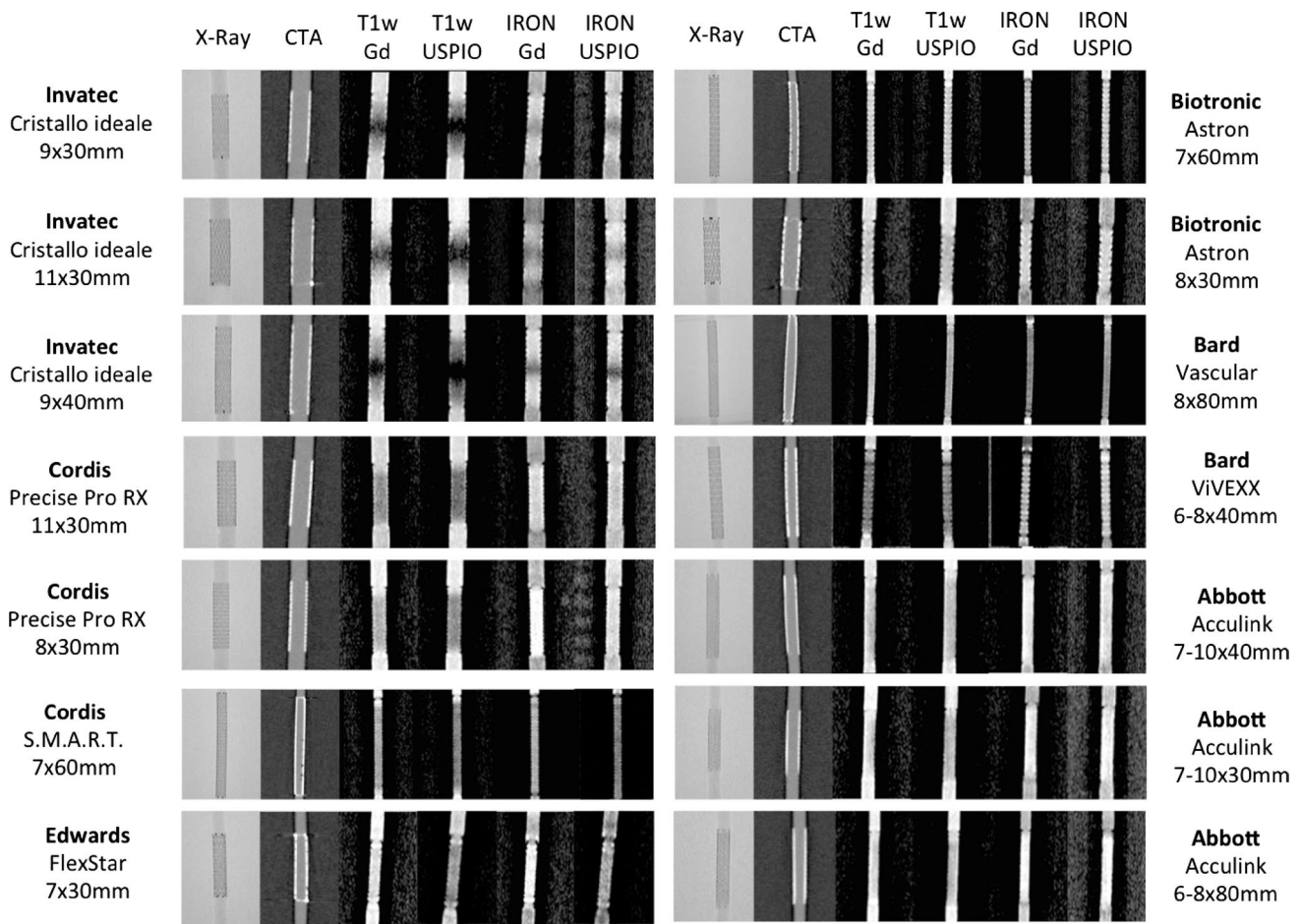


Fig. 1 Overview of contrast enhanced stent visualization for all examined stents using X-ray angiography, computed tomography angiography (CTA), conventional T1-weighted (T1w) magnetic resonance

angiography (MRA) and inversion recovery with on-resonant water suppression (IRON)-MRA

within the ‘open-close-open’ stent group compared to conventional T1w MRA (Fig. 4c, d).

Observer variabilities

Inter-(intra-)observer variabilities for CTA-based SNR and ALN were 6.2% (1.9%) and 3.0% (2.8%), respectively. For MRI-based SNR and diameter assessment inter-(intra-)observer variabilites were 6.6% (4.8%) and 7.5% (4.6%) for IRON and conventional T1w MRA, respectively.

Discussion

Assessment of peripheral in-stent lumen still remains challenging due to stent-related artifacts in MRA. In the present study we demonstrate that IRON-MRA can improve in-stent lumen assessment in vitro, and provide increased SNR, CNR and RIS as compared to conventional T1w

MRA both using Gd with clinically established parameters and USPIOs as intraluminal contrast material.

Stent-related artifacts in MRA

Stent-related artifacts, which impair stent visualization in MRA occur mainly due to susceptibility and radiofrequency shielding effects [13–15]. In our study, the artifacts in conventional T1w MRA images are more in keeping with radiofrequency shielding with the greatest signal loss in the middle of the stent. Susceptibility artifacts in nitinol stents are much weaker than in stainless-steel stents, and can be partially overcome by using a high flip angle [23]. The value of IRON-MR imaging in conjunction with USPIOs was recently demonstrated for MRA in rabbits and non-invasive detection of plaque inflammation in rabbit aortas [17, 24]. Currently, little is known on the value of the IRON-MR imaging protocols for stent visualization. In the present in vitro study, we demonstrate that IRON-MRA improves

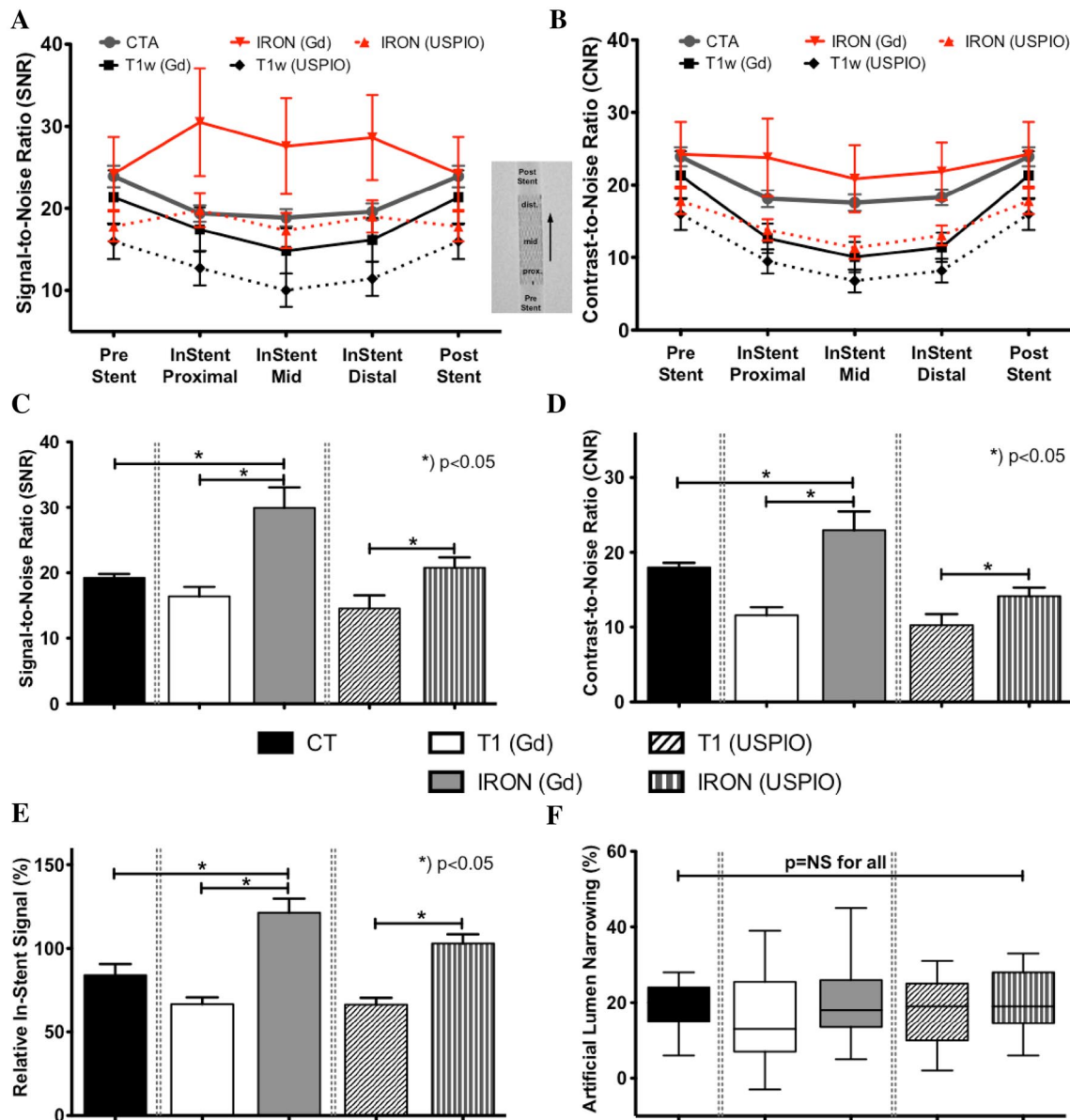


Fig. 2 SNR and CNR analysis for all stents. **a–d** Constant SNR and CNR remained or even increased within the stented tube segments using IRON-MRA, whereas conventional T1w MRA and with CTA revealed a decrease of in-stent signal and contrast. **e** IRON-MRA provides highest RIS in conjunction with Gd and USPIOs. **f** ALN was

similar for all four tested modalities. *S/CNR* signal/contrast-to-noise ratio, *T1w* T1-weighted, *IRON* inversion recovery on-resonant water suppression, *MRA* magnetic resonance angiography, *Gd* Gadolinium, *USPIO* ultrasmall superparamagnetic nanoparticles

SNR and CNR in conjunction with Gd and USPIOs as compared to conventional T1w MRA, especially for in-stent lumen segments. This is in line with previous observations on improved SNR and CNR in IRON-MR images due to off-resonance and additional signal gain due to Gd-associated T1 shortening [17, 18]. In addition, IRON-MRA may improve in-stent signal by further reduction of radio-frequency shielding artifacts, which has to be evaluated in future studies. However, IRON imaging is an order of magnitude longer than T1w imaging, which may limit its application to targeted stented vessel segments. Nevertheless, in

light of the remarkable results with Gd-enhanced IRON-MRA, the implementation of such an approach in the clinical realm appears promising.

By visual analysis, we observed three different patterns of stent-related artifacts in MRA, including (i) signal reduction in the mid of the stent, (ii) symmetric signal loss at the stent ends, and (iii) signal void around the stent struts which is in accord with previous investigations [11]. IRON-MRA provided an increased in-stent signal in conjunction with both Gd and USPIOs, while amplification of the above artifact patterns occurred in conventional T1w MRA. However, flip

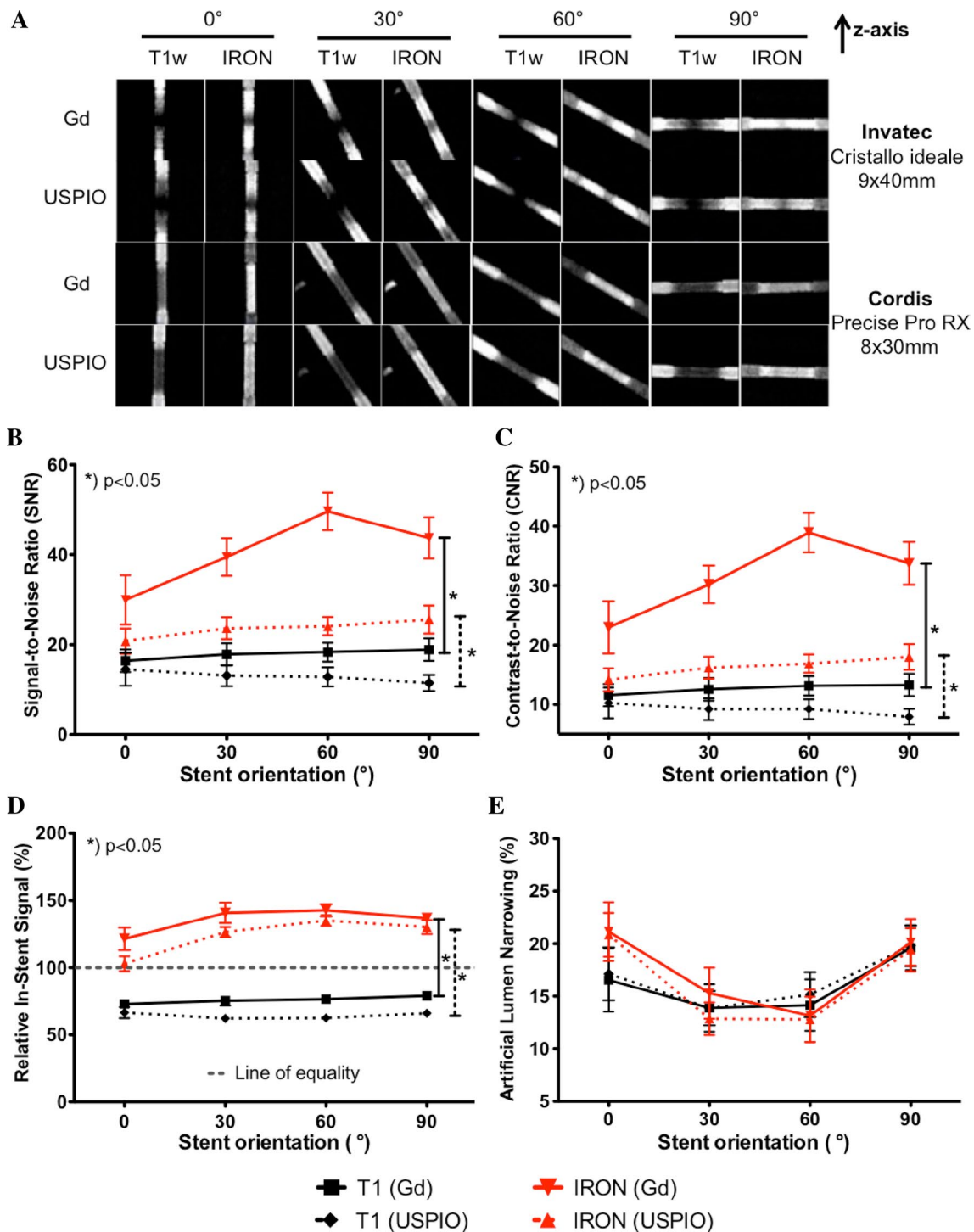


Fig. 3 Representative MRA images of stents with an ‘open-close-open’ strut design (Invatec) and ‘open’ strut configuration (Cordis) in different orientations relative to the main magnetic field B_0 , z-axis. **a** IRON-MRA provides significant improvement of in-stent visualization for the ‘open-closed-open’ strut design. **b–d** IRON-MRA in conjunction with Gd provides increase of SNR, CNR and RIS at 30°

and 60° compared to 0° and 90°, whereas values remained constant with different angles for the T1-weighted images (average values for all stents). **e** Artificial lumen narrowing (ALN) decreased at 30° and 60°, without reaching significant difference between all tested imaging approaches. *MRA* magnetic resonance angiography, *IRON* inversion recovery with on-resonant water suppression

angle was higher in the applied IRON-MRA as compared to the conventional T1w sequence protocol, which may cause an additional increase of in-stent signal due to reduction of

radiofrequency shielding effects in IRON-MR images. Nevertheless, signal loss at the stent ends and signal void surrounding the stent struts were comparable in conventional

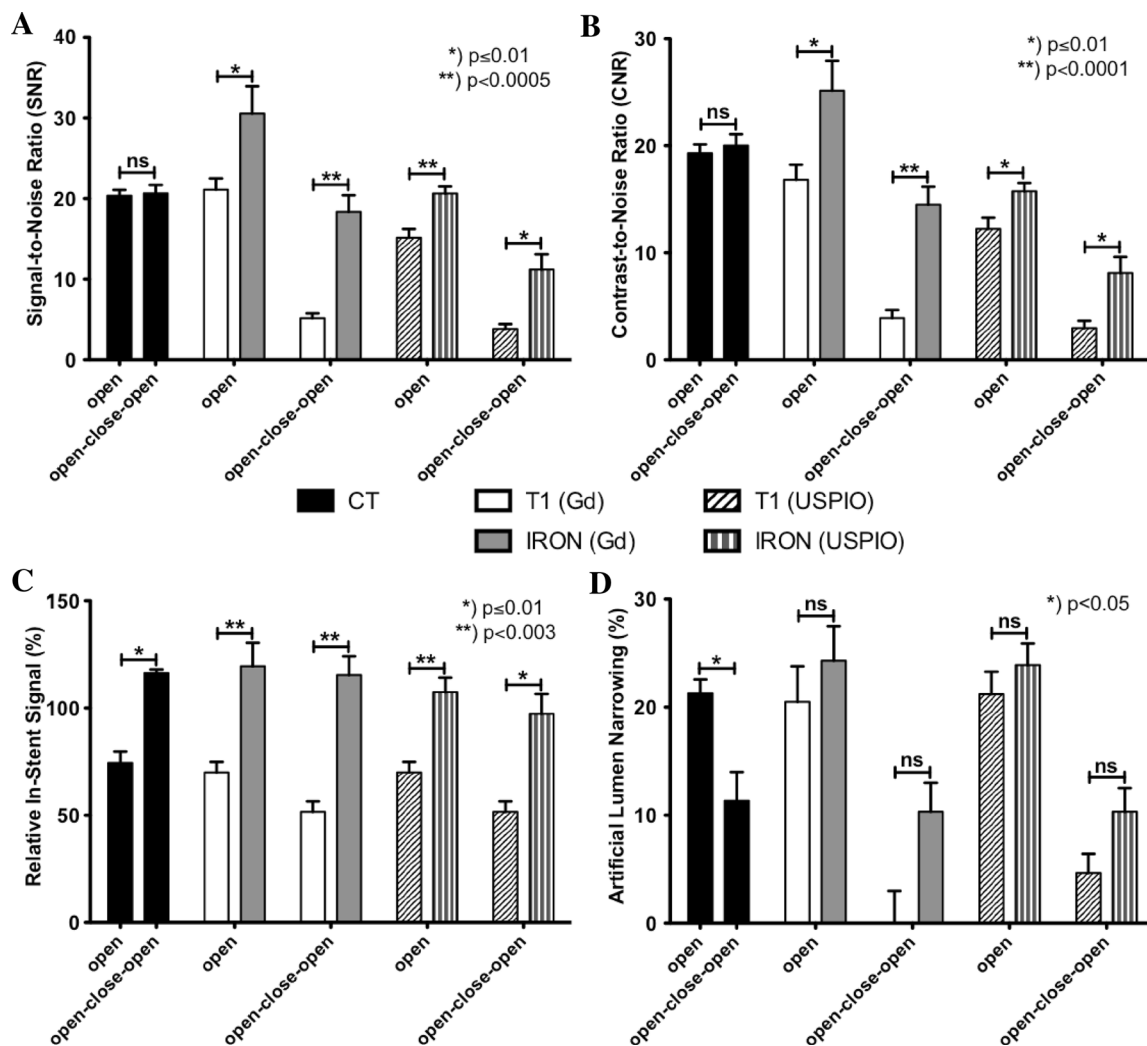


Fig. 4 Investigation to assess the impact of stent design ('open' versus 'open-close-open') on MRI-based visualization. **a–c** Both Gd- and USPIO-enhanced IRON-MRA provides remarkable improvement of SNR, CNR and RIS for stents with an 'open-close-open' configuration.

d T1-weighted and IRON-based MRA provide comparable ALN values. *MRA* magnetic resonance angiography, *IRON* inversion recovery with on-resonant water suppression

T1w and IRON-MRA, suggesting that these two artifact patterns could mainly occur due to radiofrequency effects. In this context, there is still controversy on the role of dedicated MR imaging protocols for the improvement of ALN [11, 25, 26]. Despite the significant improvement of RIS by IRON-MRA, we observed similar ALN in all tested modalities. These results underline the hypothesis of susceptibility-associated in-stent signal decrease in conventional T1w MRA, whereas radiofrequency effects may cause signal void around the stent struts and the stent ends [12].

Prior studies demonstrated an advantage of nitinol stents compared to cobalt alloy stents or bare metal stents for MR imaging [13, 27]. Using IRON-MRA for visualization of bare metal stents, artifacts due to partial volume averaging may occur. However, the value of IRON-MRA for the visualization of such non-nitinol stents merits further

investigation in future studies. Since both susceptibility and radiofrequency artifacts considerably depend on the surrounding tissue and the blood inside the stent, further in vivo investigations are needed to compare the value of conventional T1w and IRON-MRA for stent visualization.

Stent orientation

Previous investigations demonstrated the impact of stent orientation relative to the static magnetic field B_0 on stent-related artifacts with MRA [13, 23, 28]. Quantification analysis in our study revealed a weak association between SNR, CNR and RIS and stent orientation for conventional T1w MRA. Even though Gd and USPIO-enhanced IRON-MRA provided the highest SNR, CNR and RIS, the strongest orientation dependence of signal behavior was detected for

Gd-enhanced IRON-MRA with a significant signal increase at 60° orientation relative to the static magnetic field B_0 . This could be of advantage for imaging stents in strongly tortuous arteries (for example iliac or brain arteries) by IRON-MRA in conjunction with the clinically approved and widely established Gd contrast agent. This would provide steadily increased CNR with changing vessel orientation while being independent of local blood-flow.

Stent geometry and design

Especially, for nitinol stents it is well recognized, that they are significant radiofrequency shields with variation due to cell design and size. In this line, we observed a weak but negative association for in-stent signal in both conventional T1w and IRON-MRA with increasing stent diameter. Although, this is in contrast to previous reports [11], this observation could be related to the specific ROI positioning for signal assessment, which can vary along the stent axis. While SNR and CNR increased in conventional T1w MRA, IRON-MRA images exhibited no association with increasing stent length. These effects could result from both susceptibility- and radiofrequency shielding-associated decrease of in-stent signal in conventional T1w MRA images, which should get more evident with smaller stent lengths.

Apart from stent geometry, we observed that architecture of the stent struts ('open-close-open' vs. 'open') is of particular importance for the resultant image quality and the in-stent signal. The influence of the complex stent configuration on stent-related artifacts is difficult to predict in an in vitro and in vivo setting [11, 23]. In this regard, previous studies demonstrated a complete in-stent signal loss for closed cell stents with contrast-enhanced conventional MRA [29]. Along the same line, we also observed markedly decreased SNR, CNR, RIS and ALN in stents with an 'open-close-open' configuration compared to stents with 'open' stent design. In contrast, Gd-enhanced IRON-MRA exhibited an obvious improvement of image quality, SNR, CNR and RIS in comparison to conventional T1w MRA in stents with 'open-close-open' configuration.

X-ray and CTA imaging

Invasive X-ray imaging which used to be the clinical gold standard for lumen assessment of peripheral arteries is associated with a relevant procedural risk for vascular complications [30]. The administration of iodinated contrast material with X-ray or CTA is associated with potentially nephrotoxic and thyroid-related complications. For CTA, great technical efforts have been achieved in the past years to reduce stent-related artifacts (for example partial volume averaging). In the present study we used XCD kernel and a window width of 1200 HU at window level of 300 HU

to achieve improved image quality and lower ALN with the clinical 256-slice CT scanner [19]. Compared to conventional T1w MRA, CTA exhibited higher SNR and CNR, as well as RIS, the latter without reaching statistical significance. Surprisingly, Gd-enhanced IRON-MRA revealed highest SNR, CNR and RIS values, while no difference was observed in terms of ALN when compared to CTA. Since factors governing SNR in real patients is different for CTA than MRA (for example attenuation vs. coils used, specific tissue properties) it requires further in vivo studies to investigate the role of IRON-MRA and CTA in humans.

Safety of Gd and iron-based contrast material

In the past years several investigations reported that intravenous application of Gd might lead to an accumulation in certain brain structures [31–34]. However, the mechanism of neuronal Gd deposition and its clinical relevance still remain unclear. More, the chemical structure of the Gd-based contrast agent seems to be directly related to Gd accumulation, especially after repeated administrations of ionic-linear chelates [35, 36]. Very recently, Kromrey et al. [37] demonstrated that there is no evidence of neuronal Gd deposition in a 5-year follow-up after a single high-dose administration of a macrocyclic Gd-based contrast agent. Iron-based contrast materials (USPIOs) are not routinely administered in the clinical realm, however, these contrast materials are in general considered to be safe.

Minor changes in PTT (partial thromboplastin time) have been reported for iron-based contrast agents without leading to clinically significant bleeding [38]. In general, iron-based contrast material is well tolerated without significant side effects in human trials [39] and may represent a valuable alternative for contrast-enhanced MRA [40].

Limitations

Our study has some limitations. First, all experiments were conducted in vitro using a static phantom without a simulation of vessel calcification, blood flow or motion, implicating the need of further investigations to test the clinical benefit of IRON-MRA in stented vessel segments. However, in light of the improved results with Gd-enhanced IRON-MRA with clinically established parameters, its implementation in clinical imaging protocols appears promising. Second, no negative test was performed to assess the performance of conventional T1w and IRON-MRA in case of complete lumen blockage. Flip angle was higher in the IRON-MRA as compared to the conventional T1w imaging protocol, which may impact on the improved in-stent signal in IRON-MRA images. Quantification analysis on the extent of stent-related susceptibility artifacts and the role of stent strut thickness was not investigated in this study.

Only nitinol stents were included in this study because they represent the mostly used stents in invasive treatment of peripheral artery disease. Since the presented results cannot be generalized to all stents with different material further studies will be warranted to investigate the role of IRON-MRA for imaging of cobalt alloy or stainless steel stents. Finally, we used relatively low intraluminal concentrations of Gd and USPIO contrast material to allow for comparison between the different MRA imaging protocols.

Conclusions

IRON-MRA improves in-stent visualization of peripheral nitinol stents in vitro compared to conventional T1w MRA both using Gd and USPIOs as contrast material. In light of these results, the clinical implementation of Gd-enhanced IRON-MRA appears promising.

Funding None.

Compliance with ethical standards

Conflicts of interest None.

References

- Fowkes FG, Rudan D, Rudan I et al (2013) Comparison of global estimates of prevalence and risk factors for peripheral artery disease in 2000 and 2010: a systematic review and analysis. *Lancet* 382:1329–1340
- Laird JR, Katzen BT, Scheinert D et al (2010) Nitinol stent implantation versus balloon angioplasty for lesions in the superficial femoral artery and proximal popliteal artery: twelve-month results from the RESILIENT randomized trial. *Circ Cardiovasc Interv* 3:267–276
- Laird JR, Katzen BT, Scheinert D et al (2012) Nitinol stent implantation vs. balloon angioplasty for lesions in the superficial femoral and proximal popliteal arteries of patients with claudication: three-year follow-up from the RESILIENT randomized trial. *J Endovasc Ther* 19:1–9
- Layden J, Michaels J, Birmingham S, Higgins B, Guideline Development G (2012) Diagnosis and management of lower limb peripheral arterial disease: summary of NICE guidance. *BMJ* 345:e4947
- Norgren L, Hiatt WR, Dormandy JA et al (2007) Inter-Society Consensus for the Management of Peripheral Arterial Disease (TASC II). *J Vasc Surg* 45(Suppl S):S5–S67
- Davenport MS, Khalatbari S, Cohan RH, Dillman JR, Myles JD, Ellis JH (2013) Contrast material-induced nephrotoxicity and intravenous low-osmolality iodinated contrast material: risk stratification by using estimated glomerular filtration rate. *Radiology* 268:719–728
- Einstein AJ (2009) Radiation protection of patients undergoing cardiac computed tomographic angiography. *JAMA* 301:545–547
- Health Quality O (2010) Stenting for peripheral artery disease of the lower extremities: an evidence-based analysis. *Ont Health Technol Assess Ser* 10:1–88
- Brockmann C, Jochum S, Sadick M et al (2009) Dual-energy CT angiography in peripheral arterial occlusive disease. *Cardiovasc Intervent Radiol* 32:630–637
- Edelman RR, Storey P, Dunkle E et al (2007) Gadolinium-enhanced off-resonance contrast angiography. *Magn Reson Med* 57:475–484
- Frolich AM, Pilgram-Pastor SM, Psychogios MN, Mohr A, Knauth M (2011) Comparing different MR angiography strategies of carotid stents in a vascular flow model: toward stent-specific recommendations in MR follow-up. *Neuroradiology* 53:359–365
- Bartels LW, Bakker CJ, Viergever MA (2002) Improved lumen visualization in metallic vascular implants by reducing RF artifacts. *Magn Reson Med* 47:171–180
- Klemm T, Duda S, Machann J et al (2000) MR imaging in the presence of vascular stents: a systematic assessment of artifacts for various stent orientations, sequence types, and field strengths. *J Magn Reson Imaging* 12:606–615
- Maintz D, Kugel H, Schellhammer F, Landwehr P (2001) In vitro evaluation of intravascular stent artifacts in three-dimensional MR angiography. *Invest Radiol* 36:218–224
- Straube T, Wolf S, Flesser A et al (2005) MRI of carotid stents: influence of stent properties and sequence parameters on visualization of the carotid artery lumen. *Rofa* 177:375–380
- Stuber M, Gilson WD, Schar M et al (2007) Positive contrast visualization of iron oxide-labeled stem cells using inversion-recovery with ON-resonant water suppression (IRON). *Magn Reson Med* 58:1072–1077
- Korosoglou G, Shah S, Vonken EJ et al (2008) Off-resonance angiography: a new method to depict vessels—phantom and rabbit studies. *Radiology* 249:501–509
- Vonken EJ, Korosoglou G, Yu J, Schar M, Weissleder R, Stuber M (2009) On the dual contrast enhancement mechanism in frequency-selective inversion-recovery magnetic resonance angiography (IRON-MRA). *Magn Reson Med* 62:314–324
- Steen H, Andre F, Korosoglou G et al (2011) In vitro evaluation of 56 coronary artery stents by 256-slice multi-detector coronary CT. *Eur J Radiol* 80:143–150
- Etienne A, Botnar RM, Van Muiswinkel AM, Boesiger P, Manning WJ, Stuber M (2002) “Soap-Bubble” visualization and quantitative analysis of 3D coronary magnetic resonance angiograms. *Magn Reson Med* 48:658–666
- Maintz D, Seifarth H, Raupach R et al (2006) 64-slice multidetector coronary CT angiography: in vitro evaluation of 68 different stents. *Eur Radiol* 16:818–826
- Hahnel S, Trossbach M, Braun C et al (2003) Small-vessel stents for intracranial angioplasty: in vitro comparison of different stent designs and sizes by using CT angiography. *AJNR* 24:1512–1516
- Wang Y, Truong TN, Yen C et al (2003) Quantitative evaluation of susceptibility and shielding effects of nitinol, platinum, cobalt-alloy, and stainless steel stents. *Magn Reson Med* 49:972–976
- Gitsioudis G, Stuber M, Arend I et al (2013) Steady-state equilibrium phase inversion recovery ON-resonant water suppression (IRON) MR angiography in conjunction with superparamagnetic nanoparticles. A robust technique for imaging within a wide range of contrast agent dosages. *J Magn Reson Imaging* 38:836–844
- Lettau M, Sauer A, Heiland S, Rohde S, Bendszus M, Hahnel S (2009) Carotid artery stents: in vitro comparison of different stent designs and sizes using CT angiography and contrast-enhanced MR angiography at 1.5 T and 3 T. *AJNR* 30:1993–1997
- Lettau M, Sauer A, Heiland S et al (2010) In vitro comparison of different carotid artery stents: a pixel-by-pixel analysis using CT angiography and contrast-enhanced MR angiography at 1.5 and 3 T. *Neuroradiology* 52:823–830
- Kuehne T, Saeed M, Moore P et al (2002) Influence of blood-pool contrast media on MR imaging and flow measurements in

- the presence of pulmonary arterial stents in swine. *Radiology* 223:439–445
28. Bunck AC, Juttner A, Kroger JR et al (2012) 4D phase contrast flow imaging for in-stent flow visualization and assessment of stent patency in peripheral vascular stents—a phantom study. *Eur J Radiol* 81:e929–e937
 29. Hahnel S, Nguyen-Trong TH, Rohde S et al (2006) 3.0T contrast-enhanced MR angiography of carotid artery stents: in vitro measurements as compared with 1.5T. *J Neuroradiol* 33:75–80
 30. European Stroke O, Tendera M, Aboyans V et al (2011) ESC Guidelines on the diagnosis and treatment of peripheral artery diseases: document covering atherosclerotic disease of extracranial carotid and vertebral, mesenteric, renal, upper and lower extremity arteries: the Task Force on the Diagnosis and Treatment of Peripheral Artery Diseases of the European Society of Cardiology (ESC). *Eur Heart J* 32:2851–2906
 31. McDonald RJ, McDonald JS, Kallmes DF et al (2015) Intracranial gadolinium deposition after contrast-enhanced MR imaging. *Radiology* 275:772–782
 32. Kanda T, Ishii K, Kawaguchi H, Kitajima K, Takenaka D (2014) High signal intensity in the dentate nucleus and globus pallidus on unenhanced T1-weighted MR images: relationship with increasing cumulative dose of a gadolinium-based contrast material. *Radiology* 270:834–841
 33. Kanda T, Fukusato T, Matsuda M et al (2015) Gadolinium-based contrast agent accumulates in the brain even in subjects without severe renal dysfunction: evaluation of autopsy brain specimens with inductively coupled plasma mass spectroscopy. *Radiology* 276:228–232
 34. Errante Y, Cirimele V, Mallio CA, Di Lazzaro V, Zobel BB, Quattrocchi CC (2014) Progressive increase of T1 signal intensity of the dentate nucleus on unenhanced magnetic resonance images is associated with cumulative doses of intravenously administered gadodiamide in patients with normal renal function, suggesting dechelation. *Invest Radiol* 49:685–690
 35. Radbruch A, Weberling LD, Kieslich PJ et al (2015) Gadolinium retention in the dentate nucleus and globus pallidus is dependent on the class of contrast agent. *Radiology* 275:783–791
 36. Kanda T, Osawa M, Oba H et al (2015) High signal intensity in dentate nucleus on unenhanced T1-weighted MR Images: association with linear versus macrocyclic gadolinium chelate administration. *Radiology* 275:803–809
 37. Kromrey ML, Liedtke KR, Ittermann T et al (2016) Intravenous injection of gadobutrol in an epidemiological study group did not lead to a difference in relative signal intensities of certain brain structures after 5 years. *Eur Radiol*. doi:10.1007/s00330-016-4418-z
 38. Reimer P, Tombach B (1998) Hepatic MRI with SPIO: detection and characterization of focal liver lesions. *Eur Radiol* 8:1198–1204
 39. Hamm B, Staks T, Taupitz M et al (1994) Contrast-enhanced MR imaging of liver and spleen: first experience in humans with a new superparamagnetic iron oxide. *J Magn Reson Imaging* 4:659–668
 40. Neuwelt EA, Hamilton BE, Varallyay CG et al (2009) Ultras-small superparamagnetic iron oxides (USPIOs): a future alternative magnetic resonance (MR) contrast agent for patients at risk for nephrogenic systemic fibrosis (NSF)? *Kidney Int* 75:465–474